Nuclear Instruments and Methods in Physics Research B 334 (2014) 81–87

Contents lists available at ScienceDirect

Nuclear Instruments and Methods in Physics Research B

journal homepage: www.elsevier.com/locate/nimb

Optimization of BaF_2 positron-lifetime spectrometer geometry based on the Geant4 simulations

L.Yu. Dubov [b], V.I. Grafutin [a], Yu.V. Funtikov [a], Yu.V. Shtotsky [b], L.V. Elnikova [a,*]

[a] FSBI RF SSC Institute for Theoretical and Experimental Physics, Bolshaya Cheremushkinskaya 25, Moscow 117218, Russian Federation
[b] National Research Nuclear University «MEPhI», Kashirskoe Shosse 31, Moscow 115409, Russian Federation

ARTICLE INFO

Article history:
Received 10 December 2013
Received in revised form 30 April 2014
Accepted 14 May 2014

Keywords:
Positron annihilation lifetime spectroscopy
Spectrometer geometry
Geant4 simulation

ABSTRACT

Incorrect choice of measuring experimental geometry and energy windows for a positron-lifetime spectrometer with BaF_2 scintillators can lead to a significant distortion in a measured spectrum. Contribution of the distorted events for a non-optimal geometry may exceed 50%. It reduces the measured lifetimes of the spectral components and redistributes their intensities. The Geant4 simulation allows to estimate an influence of the measuring geometry on the spectrum distortion and to choose the most appropriate energy windows. The optimal geometry with a lead absorber between detectors suppresses contribution of the distorted coincidences down to 1% providing sufficiently high count rate of true events.

1. Introduction

Positron annihilation spectroscopy is a traditional method of non-destructive testing, allowing to study electronic structure of materials, mechanical and radiation-induced defects [1–3]. In a conventional positron lifetime measurements, the radioactive isotope ^{22}Na is used as a positron source. In the source, the emission of positrons is accompanied by a 1.274 MeV photon.

The emitted positrons enter the studied sample where, in several picoseconds, they are slowing down to thermal energies and eventually annihilate, emitting a pair of annihilation photons with energies of 0.511 MeV. The individual positron lifetime can be defined as the time interval between birth of a nuclear photon and birth of annihilation photons. To detect the photons fast scintillation detectors are used. So positron lifetime is measured as a time delay of the detector pulses produced by an annihilation photon (Stop signal) in relation to the detector pulses produced by a nuclear photon (Start signal).

A spectrum of time delays between detecting the 0.511 MeV and 1.274 MeV photons is called hereafter the delayed-coincidence spectrum. The delayed-coincidence spectrum is described usually by a convolution of the exponential components with the timing response function of the spectrometer. By analyzing this spectrum information about the lifetimes τ_i and the intensities I_i of various groups i of positrons annihilating in a given material can be obtained. The width of the timing response function and the delayed-coincidence counting rate are the most important parameters that limit the ability of the spectrometer in identifying and resolving positron-lifetime components in the spectrum.

An improvement of the time resolution is of utmost importance for a large number of applications of positron-lifetime spectroscopy, especially for studying positron lifetime in metallic systems with high defect concentration, where the difference between the lifetime components can be of the order of 10 ps.

Conventionally, time information is extracted from the detector pulses using constant-fraction differential discriminators (CFDDs) and a time-to-amplitude converter (TAC) whose output pulses are collected in a multi-channel analyzer (MCA) to form the lifetime spectrum.

So there are a number of random processes which influence a time delay. The first one is the propagation of nuclear and annihilation photons from the point of birth to the point (or points) of interaction in a detector. The propagation time is a random value and depends on the size of detectors, on the distance between them, on the number of the photon scattering in the detectors and environment. The second is the process of light collection in the scintillation crystal. The third is the process of pulse formation in the photo multiplier tube. The forth is the instability of thresholds in CFDD. Every element of the signal processing chain gives its contribution to the timing resolution of the PAL spectrometer.

For our purposes, it is convenient to represent the whole response function as a convolution of two partial response functions. The first part describes the emergence time of light flashes in scintillator and depends on geometrical parameters of a detector

* Corresponding author. Tel.: +7 9060862582.
E-mail addresses: Dubovl@mail.ru (L.Yu. Dubov), grafutin@itep.ru (V.I. Grafutin), yshtotsky@mail.ru (Yu.V. Shtotsky), elnikova@itep.ru (L.V. Elnikova).

http://dx.doi.org/10.1016/j.nimb.2014.05.006
0168-583X/

system. Therefore we call it *the geometrical response function*. The second one is concerned with the time dispersion in the detectors and the signal processing chain. We call it *the apparatus response function*. In this work only geometrical part is simulated and discussed in detail. The apparatus part meanwhile is approximated by the normal distribution with FWHM typical for the available lifetime spectrometer (275 ps) to compare the simulation results with the experimental data.

There are many works associated with the problem of improving the time resolution of the lifetime spectrometer [4–7]. Many authors note, that the γ-rays detection in the positron lifetime spectrometer is generally accompanied with undesired effects whose intensities depend on the scattering efficiency and a solid angle covered by the scintillators. The detection of backscattered γ-rays leads to detection of undesired "false" coincidences. The similar undesired effect occurs when a new photo multiplier pulse is detected on the tail of a previous one. This effect is well-known as a pileup. But we do not consider a pileup here.

The number of "false" coincidences depends primarily on the geometry of the detector system. For instance, the maximal number of parasitic events is observed in the traditional face-to-face geometry with the sandwiched ^{22}Na source located at the detectors common axis.

In some cases, the distortion of the experimental spectrum cannot be compensated by the conventional software used for processing the lifetime spectra. To obtain lifetimes and intensities from the experimental spectrum, the invariability of the time response function for the entire range of signal delays is supposed. But it is not true for some arrangements of the source-sample-detectors system due to parasitic effects. Using such arrangements may result in the significant distortion of the lifetime spectrum and hence can lead to errors in determining lifetimes τ_i and intensities I_i of the components.

To choose the optimal arrangement of the source-sample-detectors system and energy windows, that provide the minimal distortion of the spectrum with an acceptable rate of the undistorted coincidences, we have analyzed the shape of the geometrical response function basing on the Monte Carlo simulation.

2. Simulation method

The simulation of positron lifetime spectrometer described here is based on GEANT4 [8] used via the GATE simulation environment [9] and the Matlab toolkit. It takes advantage of GEANT4's capabilities for modeling the setup as well as transport of beta particles and γ-rays and their interactions with matter. It also takes advantage of the Matlab data structures for efficient processing of the GEANT's track data. The tools provided by each package allow the flexibility in adjustment of the simulation parameters at the run time as well as an efficient storage, inspection and processing of simulated data and comparison with an experimental spectra.

The simulated setup includes two cylindrical BaF_2 scintillators with a diameter of 25.7 mm and a height of 12.9 mm as detectors. The detectors may be placed at different distances (L_1 and L_2) from the center of the spectrometer opposite each other or be rotated at an angle φ. A plane isotropic source with a diameter of 5 mm is placed between them at a height h from the horizontal axis. Besides the geometrical elements indicated in Fig. 1 the model also included aluminum shells of the detectors.

Typically for every arrangement of simulated setup 10 millions of source decays are generated. For ^{22}Na, nuclear photon and positron are generated for the each decay in the source, with their parameters, such as the time, the momentum and the energy. Then two annihilation photons are emitted as a result of the positron annihilation. In the case of ^{60}Co, two nuclear photons are generated for the each decay.

An elementary trajectory step (referred to in Geant4 simply as a step) is applied. A step corresponds to the trajectory of a particle between discrete interactions. We consider the photoelectric effect, the coherent and Compton scattering for photons and the multiple scattering, the ionization, the bremsstrahlung for positrons and electrons. During a step the changes for the particle's energy and momentum are calculated. The length of a step depends upon the nature of interaction, the type of particle and material, etc. The details for the step parameters calculation can be found in [8].

In Geant4, information about the single physical interaction within specified sensitive regions of a detector is saved as a hit. The information given by a hit is the position and time of the interaction, momentum and energy of the track, the energy deposition of the step, the interaction type of the hit.

Thus for each photon interaction within scintillation crystal we know time and the deposited energy. If there are several photon interactions within the sensitive volume, the time of the signal is calculated as the average time weighted by the energy. The amount of energy deposited in a crystal is summed and analyzed as the amplitude of the detector signal.

As a result, a set of signals is simulated for two sensitive volumes (Start and Stop detectors). Each signal is characterized by 4 parameters: the energy, the time, the decay index, the detector index. These parameters allow us to calculate the set of delayed coincidences. If the decay indexes for Start and Stop signals are the same, the event is classified as a coincidence and the time delay is calculated as the difference between times of the Stop and Start signals. In such a way, the array of time delays and two corresponding arrays of energies for the Start and Stop signal can be obtained.

The histogram of the delay array for ^{60}Co represents the prompt coincidence peak. For ^{22}Na source to emulate the lifetime, positron is generated in a fixed time τ after a nuclear photon, and the delay histogram in this case represents the geometrical response function for the fixed lifetime τ. If positron emission time is chosen randomly from the lifetime distribution, the delay histogram represents the whole lifetime spectrum blurred by the geometrical response function. To filter and classify delayed coincidences, their hits history has to be analyzed.

3. Analysis of distribution of delayed coincidences

To explain the shape of the geometrical response function for the delayed coincidence obtained with ^{22}Na source, we have to consider three successively emitted γ-rays: one nuclear photon (1.28 MeV) and two annihilation photons (0.511 MeV each). Each of these three photons can be detected either by one or by two detectors.

We consider a signal from the detector as the one-vertex event, when a light flash in the scintillator is produced by a single photon, and as the two-vertex, when one flash in the scintillator is produced by two photons together. There are three- and four-vertex events as well. If only one and two-vertex physical events in the scintillators are taken into account there are 65 possible combinations which can produce a coincidence of the Start- and Stop-signals. All combinations may be divided into four types (see Fig. 2): the "true" delayed coincidences (A-type), the "self-coincidences" (B-type), the "shifted" coincidences (C-type) and the "mixed" coincidences (D-type).

The coincidences of the A-type are "true" coincidences of signals from a nuclear photon (1.28 MeV) in the Start-detector and one of annihilation photons, delayed by time interval τ, in the Stop-detector. The only reason of the broadening of the A-type coincidences peak is the difference between distances traveled by

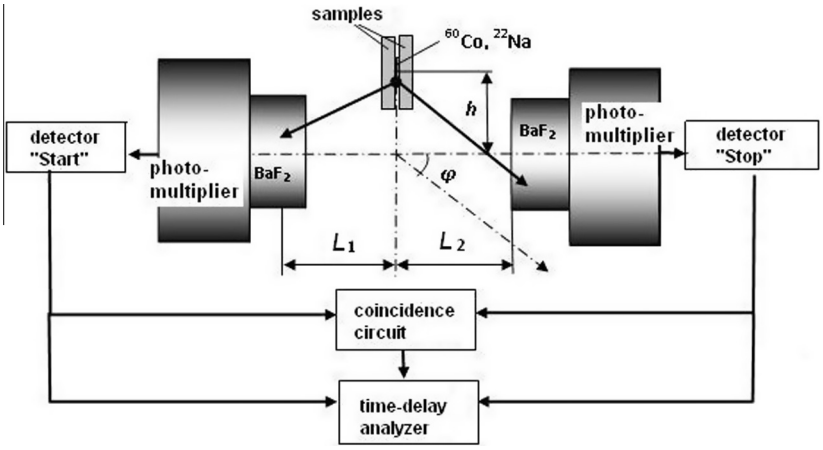

Fig. 1. The block diagram of a lifetime spectrometer.

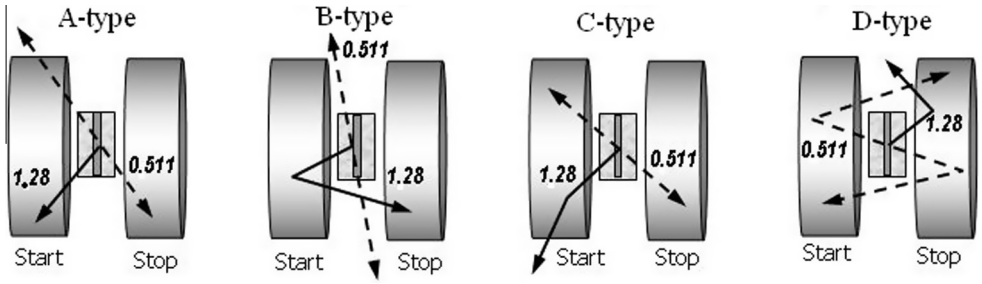

Fig. 2. Typical combinations of events for different types of coincidences from ^{22}Na.

photons to the points of an interaction. The mean delay for A-type coincidences depends only on the positron lifetime τ.

Coincident signals in both detectors can be also produced either by the single nuclear photon only or by the pair of annihilation photons only. Such coincidences are attributed to "self-coincidence" (B-type). For this type the delay distribution consists of three peaks. The peak in the zero channel is a result of a registering one annihilation photon by the Start detector and another by the Stop detector. Two shifted peaks are attributed to the case when a single nuclear photon is registered in both detectors. These peaks are shifted relatively to the zero channel by the time $\pm\Delta t$, which depends on the distance between the detectors. A delay for the B-type coincidences does not depend on the positron lifetime τ.

The C-type coincidences occur, when one of detectors registers the nuclear and annihilation photons together. It results in the later triggering in the Start-channel or to an earlier triggering in the Stop-channel because the annihilation photon is delayed by the time τ. The response time t^* of a channel was defined as the energy weighted average: $t^* = (t_n E_n + t_a E_a)/(E_n + E_a)$, where t_n and t_a are the registration times for the nuclear and annihilation photons respectively, while E_n and E_a are the energies absorbed in the scintillator. Thus, the time delay for the C-type coincidences can be varied from 0 to τ.

Coincidences of the D-type are caused by double or triple events with time shifts Δt, τ, or $\tau + \Delta t$. As a result, the delays for the D-type coincidences may vary in a range from $-\tau$ to $\tau + \Delta t$.

To minimize a distortion of the experimental lifetime spectrum, it is necessary to choose a measuring geometry and optimal values for energy windows, which provide minimal contribution of the "B–D" types of coincidences, while retaining an acceptable counting rate for the A-type coincidences.

For simulation of the lifetime spectra, the same algorithm as for the fixed lifetime is used. The positron generation time is taken from the ideal lifetime distribution as a random value. The ideal lifetime distribution is described as the sum of exponential components. Using the Geant4 simulation, the lifetime spectrum blurred by the geometrical response function can be obtained. To simulate the experimental spectrum, this delay distribution have to be blurred by the apparatus response function yet (the normal distribution with a FWHM = 275 ps in our case). A simulated lifetime spectrum is obtained from an array of simulated delays by a histogram and taking into account the width of the spectrum analyzer's channel (5 ps). Then the simulated spectrum is processed and the inverse problem is solved using the Palsfit software [10]. Results of the processing have to be compared with initial lifetimes and intensities of components.

4. Results and discussion

Simulations were carried out for five different geometries (see Table 1). Geometry #1 (the detectors are placed at 10 mm from

Table 1
Contributions of the groups of coincidences into delayed coincidence spectrum and a number of "true" coincidences of the A-type (by 10^6 positrons) for different measuring geometries at the thresholds of the differential discriminator "Start" 0.7 ÷ 1.4 MeV and "Stop" 0.35 ÷ 0.60 MeV.

Measuring geometry (L_1-L_2-h), mm			Contribution of coincidences, %				$N_{«A»}$
			A	B	C	D	
110-10-20-Pb	#1	Start Pb Stop	99.5	0.3	0.2	0	115
10-10-20	#2	Start Stop	96.4	1.1	0.3	2.2	241
0-0-20	#3	Start Stop	70.4	20.8	0,5	8.3	344
10-10-0	#4	Start Stop	72.7	0.5	23.9	2.9	345
0-0-0	#5	Start Stop	61.5	1.5	24.5	12.5	3041

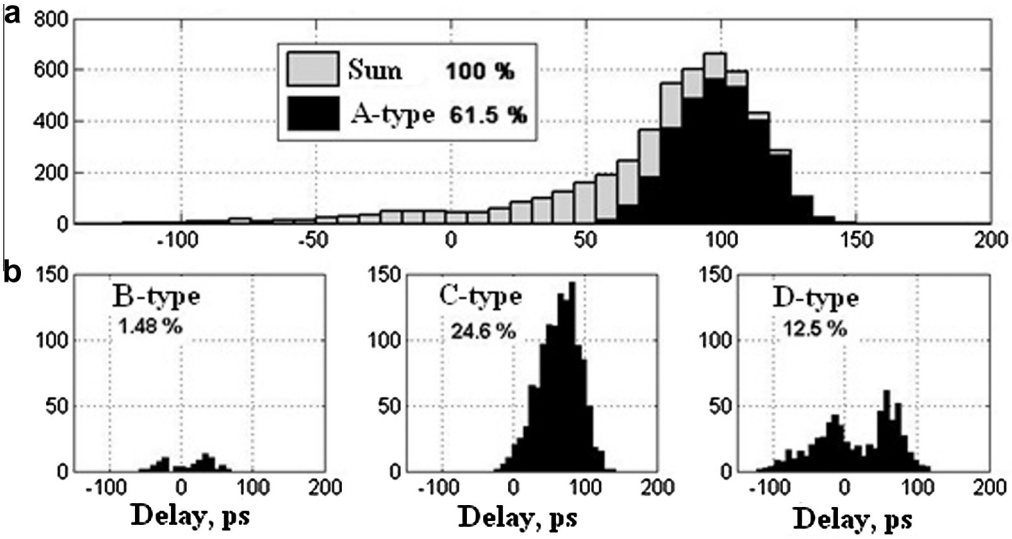

Fig. 3. The distribution of the delay time for ^{22}Na, $\tau \sim 100$ ps, $L_1 = L_2 = h = 0$, at the energy windows «Start»: 0.7–1.4 MeV and «Stop»: 0.35–0.6 MeV; (a) all the coincidences and the A-type "true" coincidences; (b) the B-, C-, and D-type coincidences.

the center [$L_1 = L_2 = 10$ mm], the thickness of the lead shield is 10 mm, the source is shifted by $h = 20$ mm relatively to the central axis) is the optimal configuration. Geometry #5, commonly referred to as "face to face" (the closest distance between the detectors and the "central" position of the source) is traditional.

Every geometry under our study showed differences in the geometrical response function defined by various contributions of the A–D coincidence events.

Fig. 3 shows the delay distributions for the A-, B-, C-, and D-types of coincidences and the total peak ($\Sigma = A + B + C + D$) for the case when the lifetime τ of an each positron is100 ps. For the A-type coincidences, a symmetric Gauss-like distribution with the $FWHM_A \approx 50$ ps is observed. The width of this distribution does not depend on the positron lifetime. The distribution of "self-coincidences" of the B-type consists of three peaks: a central peak and two symmetrically shifted ($\Delta t = \pm 40$ ps) lateral peaks with $FWHM_B \approx 30$ ps. The delay distribution of the C-type is non-symmetrical with a peak at about 75 ps with $FWHM_C \approx 60$ ps and its left side extends to the zero channel. The time distribution of the D-type is even greater biased and extends from $-\tau$ to $+\tau$. The total spectrum for all coincidences, as shown in Fig. 3a, is essentially non-symmetrical and stretched significantly in the direction of a lower lifetime.

Fig. 4 shows a shape of the total spectra for various lower thresholds of the Stop-channel from 0.15 MeV to 0.45 MeV. The spectrum distortion at the low threshold increases dramatically.

Fig. 5 demonstrates shapes of the total spectra for various fixed value of τ from 0 to 600 ps. When the positron lifetime increases, the peak position is shifted in accordance with the value of τ, while, the left part of the peaks is stretched up to $-\Delta t$. The shape of the geometrical response function in this geometry depends significantly on the positron lifetime τ.

Fig. 6 shows the amplitude diagrams for the A-, B-, C- and D-types of coincidences for non-shifted ($h = 0$ mm) and shifted ($h = 20$ mm) positions of the positron source.

The diagrams show that "self-coincidences" (B-type) are completely excluded, if the sum of the Start- and Stop-channel's lower thresholds exceeds 1.28 MeV. The "distorted" (the C- and D-type) coincidences survive under any energy thresholds, but their number can be significantly reduced by the source displacement. The number of "true" (the A-type) coincidences is determined by the width and position of the energy windows.

The results of simulations (Table 1) show that the count rate for the proposed measuring geometry #1 is much less than for the traditional "face to face" geometry (the number of "true" A-type coincidences is about 20 times less). However, the contribution of "true" coincidences for the geometry #1 is close to 100% versus some 60% for the traditional geometry.

The results for the simulated one-component spectra (0.1 ns, 0.4 ns and 2.0 ns) are presented in Fig. 7. We can see that only the geometry #1 allows us to recover the lifetimes with a good accuracy (less than 1%). For other geometries, there is a significant "shortening" of the lifetime from 5% to 20%.

Fig. 8 shows the results for 2-component spectra: [0.1 ns (50%) + 0.4 ns (50%)] and [0.1 ns (50%) + 2.0 ns (50%)]. Lifetimes and intensities are recovered with good accuracy only for the optimum measuring geometry #1 (and partly for the geometry #2). For other geometries, a significant lifetime "shortening", 10% or more, is observed. In addition, there is a substantial redistribution of component intensities: the intensity of the short-lived component

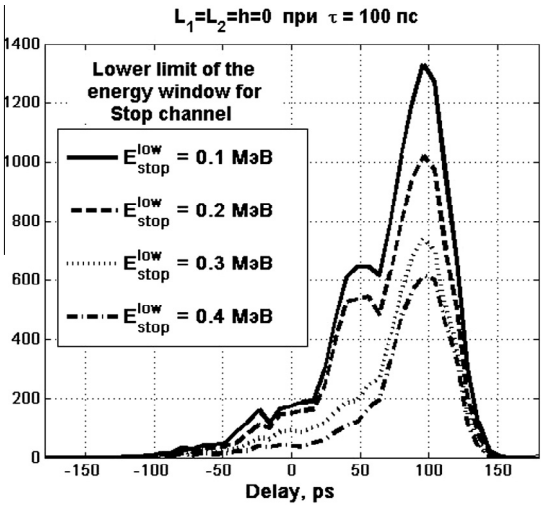

Fig. 4. The spectra for the delayed coincidences ($L_1 = L_2 = h = 0$) at the fixed $\tau \equiv 100$ ps for the lower threshold of the "Stop" channel discriminator varying from 0.1 to 0.4 MeV.

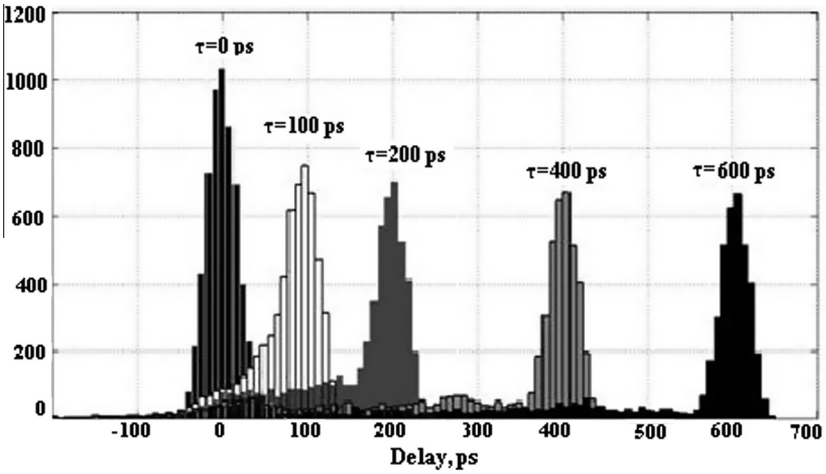

Fig. 5. The spectra of the delayed coincidences ($L_1 = L_2 = h = 0$) at $\tau = 0$, 100, 200, and 600 ps, for the thresholds of the "Stop" (0.3–0.6 MeV) and "Start" (0.7–1.4 MeV) channels.

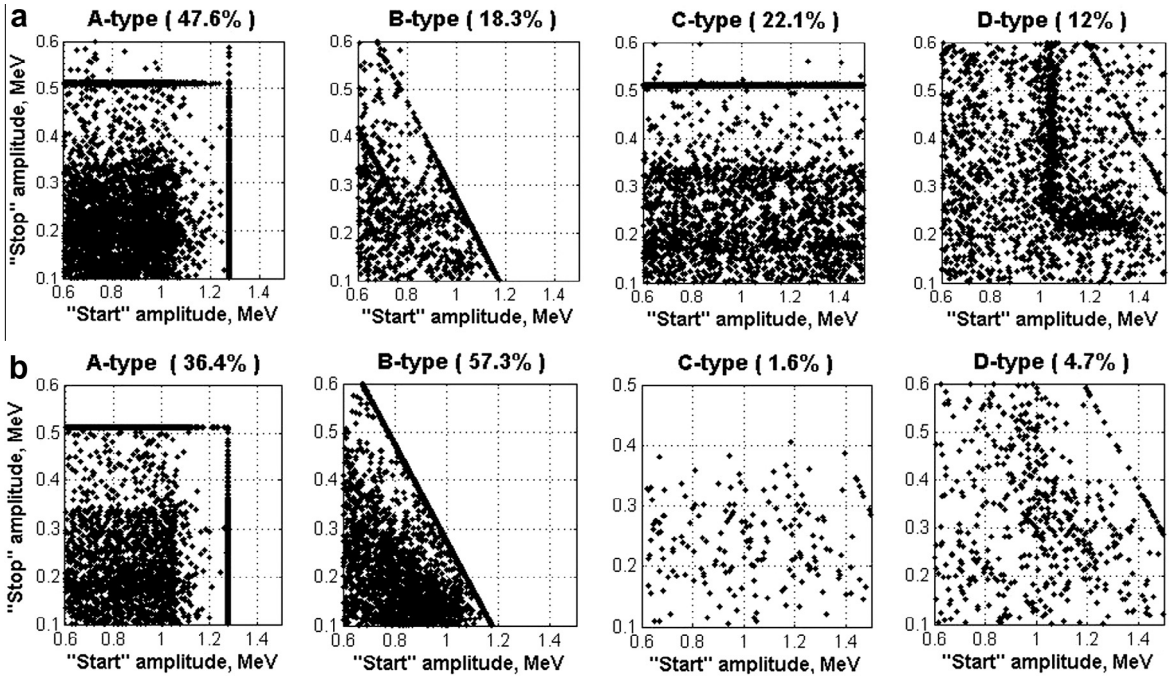

Fig. 6. The amplitude diagrams for the A-, B-, C-, and D-type coincidences (^{22}Na; "Start": 0.6–1.5 MeV; "Stop": 0.1–0.6 MeV; $L_1 = L_2 = 0$) at $h = 0$ (a) and $h = 20$ mm (b).

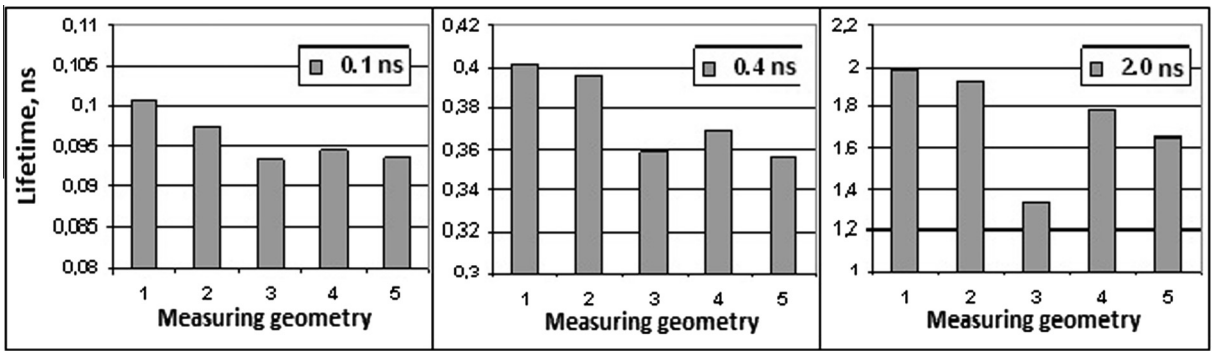

Fig. 7. The results of the processing of one-component model spectra for five different geometries (see Table 1).

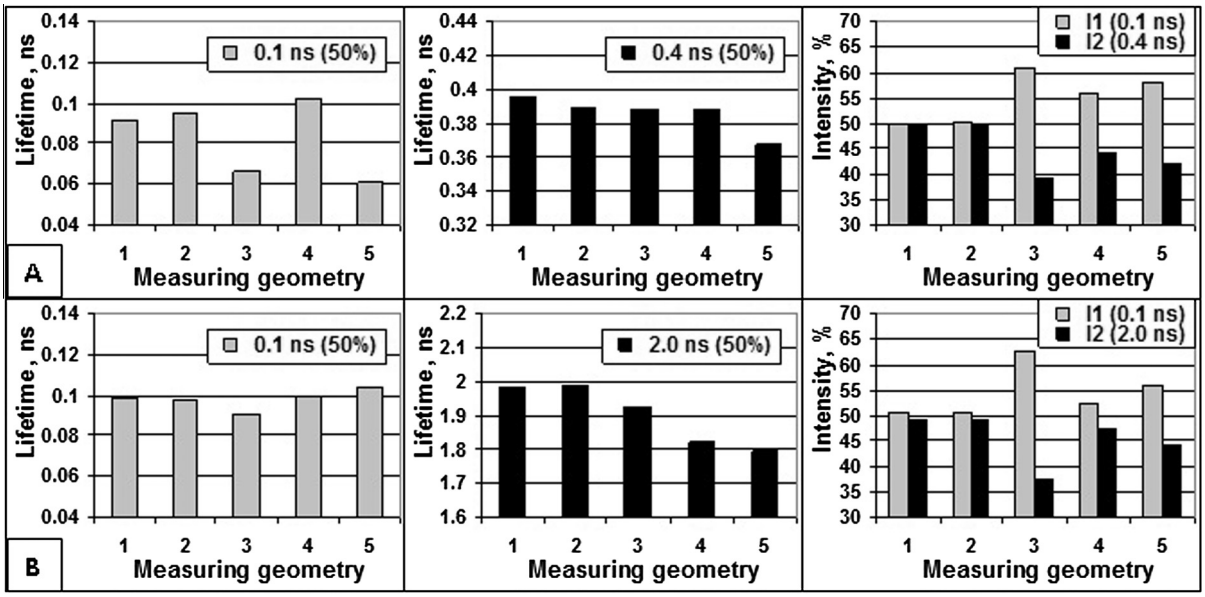

Fig. 8. The refined results of the processing of modeled two-component spectra of 0.1 ns + 0.4 ns (A) and 0.1 ns + 2.0 ns (B) by the Palsfit software with free parameters.

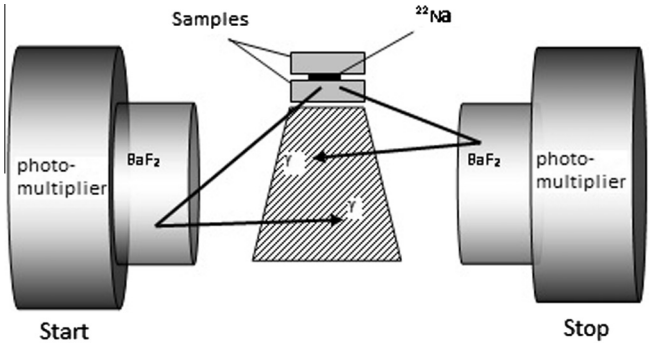

Fig. 9. The optimal measuring geometry.

increases from 50% to 60%, and the intensity of the long-lived component decreases, respectively. If the short-lived component (0.1 ns) is fixed, the long-lived component (0.4 ns or 2.0 ns) can be recovered with a good accuracy for all measuring geometries. However, the redistribution of intensities in favor of a short-living component remains.

Thus for any measuring geometries except for the optimal geometry #1 (and partly for the geometry #2), the distortion of component intensities always takes place: intensity of the short-living component increases by 10–20%, and intensity of the long-living one decreases respectively.

The results of simulations were experimentally tested on several samples with different lifetime spectra measured in various geometries [11,12]. Experiments show that long living components decrease as predicted by the model. Most clearly it was demonstrated by the long living components. So the lifetime 2.2 ns of the positronium component in *Mylar*, measured in the optimal geometry, decreases in the "face to face" geometry to 1.8 ns.

5. Conclusions

For the traditional geometry $L_1 = L_2 = h = 0$ we have the maximum count rate of the A-type ("true") coincidences ($\sim 10^3$ coincidences per 10^6 decays). However, the fraction of the B–D-type ("false") coincidences, distorting the lifetime spectrum, is greater than ~35%. It makes practically impossible a correct reconstruction of the positron lifetime distribution.

In the measuring geometry with the detectors spaced 20 mm apart ($L_1 = L_2 = 10$ mm) and with a shifted source ($h = 20$ mm), the detection efficiency of the A-type ("true") coincidences is $\sim 10^4$, but the fraction of the B–D-type coincidences decreases to 5–15%.

For the geometry with detectors rotated at 90° angle, with a lead shield arranged between the detectors, the fraction of the B–D-type coincidences is reduced to less than 2%. However, the detection effectiveness of the A-type coincidences is also less in about 3 times.

The optimal geometry, *i.e.* the shifted source and lead shield between the detectors (see Fig. 9), allows to reduce the contribution of distorting coincidences to an acceptable value.

For all measuring geometries, except the optimum one, there is a shortening of the evaluated lifetime components by 5–10% and a distortion of intensity ratio: the intensity of the short-living component increases by 10–20%, while the intensity of the more long-living component decreases respectively.

Lifetime spectra measured in a conventional "face to face" measuring geometry are significantly distorted, which leads to the "shortening" of evaluated lifetime components and to the redistribution of their intensities in favor of the short-lived components.

The proposed measuring geometry, wherein the source-sample set is shifted by 20 mm from the axis of the detector system, the scintillation detectors are spaced 10 mm apart, and the lead screen in the form of a trapezoidal prism is positioned between detectors, allows to measure an undistorted lifetime spectra and to keep an acceptable counting rate of events.

It is necessary to note that the contribution of "false" coincidences depends on efficiency of γ-ray interactions with scintillators, and our simulations show that the discussed spectrum distortion for the plastic scintillators is almost negligible.

Experimental data show that the lifetime spectra are distorted, as it is predicted by the model. The maximal distortion is observed for long-living components. For instance, the lifetime 2.2 ns of the positronium component in *Mylar*, measured in the optimal geometry, decreases in the traditional "face to face" geometry to 1.8 ns.

The proposed methodology to optimize the arrangement of a detector system is especially important for spectrometers designed for measurements with a high time resolution, but may be useful in the study of the long-living component as well.

References

[1] A. Dupasquier, A.P. Mills Jr. (Eds.), Positron Spectroscopy of Solids, IOS Press, Amsterdam, 1995.
[2] R. Krause-Rehberg, H.S. Leipner, Positron Annihilation in Solids. Defect Studies, Springer, Berlin, 1999. p. 378.
[3] V.I. Grafutin, E.P. Prokop'ev, Usp. Fiz. Nauk 172 (67) (2002) 67.
[4] F. Becvar, J. Cizek, I. Prochazka, J. Janotova, Nucl. Instrum. Methods Phys. Res. A 539 (2004) 372.
[5] T. Sharshara, M.L. Hussein, Nucl. Instrun. Methods Phys. Res. A 546 (2005) 584.
[6] F. Becvar, J. Cizek, L. Lestak, et al., Nucl. Instrum. Methods Phys. Res. A 443 (2000) 557.
[7] N. Djourelov, N. Charvin, C. Bas, et al., Nucl. Instrm. Methods Phys. Res. B 264 (2007) 165.
[8] S. Agostinelli, J. Allison, K. Amako, J. Apostolakis, H. Araujo, P. Arce, M. Asai, D. Axen, S. Banerjee, G. Barrand, et al., Nucl. Instrum. Methods Phys. Res. A 506 (2003) 250.
[9] S. Jan et al., Phys. Med. Biol. 49 (2004) 4543.
[10] J.V. Olsen, P. Kirkegaard, N.J. Pedersen, M. Eldrup, PALSfit, Risø National Laboratory, Denmark, 2006.
[11] L.Yu. Dubov, V.I. Grafutin, Yu.V. Funtikov, Yu.V. Shtotsky, MEPhI Sci. Sess. 1 (2012) 194.
[12] L. Dubov, Yu. Funtikov, V. Grafutin, D. Zvezhinskiy, Yu. Shtotsky, in: M. Roussenova, M.A. Alam, S. Dugdale (Eds.), 16th International Conference on Positron Annihilation, ICPA-16, 2012, Conference Book, Poster B. 66, p. 174.